PERGAMON

International Journal of Solids and Structures 39 (2002) 435–448

INTERNATIONAL JOURNAL OF SOLIDS and STRUCTURES

www.elsevier.com/locate/ijsolstr

Microstructure-based description for the mechanical behavior of single pearlitic colony

X. Peng *, J. Fan, J. Zeng

Department of Engineering Mechanics, School of Resources and Environmental Science, Chongqing University (A), Chongqing 400044, China

Received 3 October 2000

Abstract

A constitutive description is proposed for a single pearlitic colony based on its composition of lamellas of ferrite and cementite with a very thin interlamellar spacing. Both phases are assumed to be elastoplastic. The relationship between the increments of overall stress and strain is derived and the corresponding numerical algorithm is developed. The mechanical behavior of the colony subjected to proportional or non-proportional loading is investigated, and it shows that the overall response is anisotropic. Finite element analysis is conducted to analyze the influence of the interlamellar spacing on the mechanical response of the colony. It shows that the proposed model can not only describe the behavior of the pearlitic colony with extremely small interlamellar spacing, but also work with sufficient accuracy in the case of moderate interlamellar spacing. The constitutive response of each phase in a colony can be obtained simultaneously, which is an important step towards developing theories of microstructure-based damage and failure analysis.

Keywords: Pearlitic colony; Dual-phase lamination; Microstructure-based analysis; Constitutive equation; Cyclic plasticity

1. Introduction

Pearlitic steel is composed of numerous pearlitic colonies with randomly distributed orientations. Each colony is composed of many alternatively arranged parallel thin lamellas of ferrite and cementite. The pearlitic steel with fine lamellas possesses excellent mechanical properties such as high strength, good resistance against wear, and high fatigue life, etc. (Langford, 1977; Clayton, 1980; Hodson and Preston, 1980; Petez-Unzueta and Beynon, 1995; Sheng et al., 1998).

One of the most important properties of this kind of dual-phase materials is its locking-in interphase residual stress capability (Bower, 1989). When the material is subjected to asymmetrical stress cycling, it ratchets in the direction of mean stress, but the rate decreases gradually during the cycling. If the mean stress is then removed, the material will ratchet back in the opposite direction during the following cyclic

* Corresponding author. Fax: +86-23-65106656.
E-mail address: xhpeng@cqu.edu.cn (X. Peng).

0020-7683/01/$ - see front matter
PII: S0020-7683(01)00222-0

process, despite that the mean stress no longer exists (Bower, 1987, 1989; Bower and Johnson, 1989, 1990; Peng and Ponter, 1994a). This particular behavior accounts for the extensive use of the material for rail steel. Practically, the stress induced by rail/wheel contact is typically asymmetrical, but the ratcheting of the material is strictly limited.

A constitutive model for pearlitic rail steel was proposed by Bower (1989) and Bower and Johnson (1990), in which a new kinematic variable was introduced by modifying the model of Armstrong and Frederick (1966). It greatly improved the description of the ratcheting behavior of the pearlitic steel. Peng and Ponter (1994a) proposed a model, which separates the plastic deformation of pearlitic steel into the plastic deformation of its soft phase and the elastic–plastic deformation of its hard phase. It can describe the more complicated response of pearlitic steel, for instance, the non-vanishing steady ratcheting rate during asymmetrical stress cycling. It was shown that, assuming an elastic hard phase, this model could be reduced to Bower's model (Peng and Ponter, 1994a). A micro/macroscopic analysis for the cyclic plasticity of dual-phase pearlitic material was recently proposed by Fan (1999), taking into account the lamellar microstructure of a single pearlitic colony. A self-consistent scheme was used to obtain the macroscopic response, with which the cyclic plasticity of BS11 and the local stress evolution were analyzed.

The locking-in interphase residual stress capability and the plastic shakedown behavior of the dual-phase material are closely related to the interaction between its two phases. In order to have an insight of the particular macroscopic behavior, it is necessary to deeply understand the response of a single pearlitic colony and its microstructural dependence.

In this paper, starting from the lamellar microstructure, a description for a single pearlitic colony is obtained by assuming both ferrite and cementite phases being elastoplastic. The relationship between incremental stress and strain, and the corresponding numerical algorithm are derived. The predicted behavior of a single pearlitic colony subjected to proportional and non-proportional loading is investigated. It is shown that the overall constitutive response is, in general, anisotropic due to the interaction between the two phases. Finite element analysis is employed to study the influence of the interlamellar spacing on the response of the colony. It can be seen that, the proposed model can not only describe the behavior of a pearlitic colony with extremely small interlamellar spacing, but also predict with sufficient accuracy the behavior of a colony with moderate interlamellar spacing. The constitutive response of the ferrite and cementite phases in a colony can be obtained simultaneously, which is important for the development of a microstructure-based damage and failure analysis.

2. Constitutive equation for elastoplastic media

As shown in Fig. 1, a pearlitic colony is composed of many fine lamellas of cementite and ferrite. In Fig. 1(a) the material was taken from the head of a rail which was on-line and full-length directly quenched after

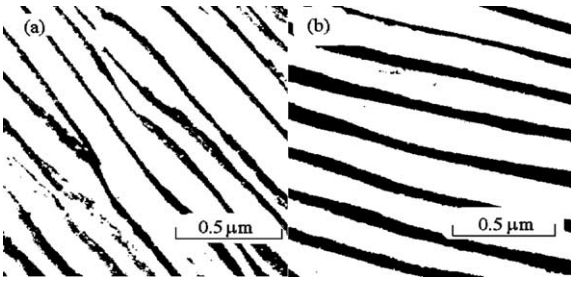

Fig. 1. The observed microstructure of a pearlitic steels: (a) quenched directly after rolling; (b) hot rolled.

rolling, while the material in Fig. 1(b) was taken from the head of a hot-rolled rail. It is clear that the orientations of lamellas are almost identical. The average interlamellar spacing in Fig. 1(a) is around 136 nm while it is around 190 nm in the other case (Fig. 1(b)). The corresponding average sizes of both pearlitic colonies are about 13 μm in diameter.

In pearlitic steel, ferrite phase serves as the soft phase while cementite represents the hard phase. The strength of cementite is much higher than that of ferrite. The mechanical behavior of a pearlitic steel depends strongly on that of cementite although the volume fraction of cementite V is only about 15%. It has been found that the plastic deformability and the failure mode of cementite are closely related to the thickness of cementite lamella. Langford (1977) pointed out that there is no evidence for gross plastic deformation of cementite plates thicker than 0.1 μm, and there is no evidence for extensive, brittle fragmentation of cementite plates thinner than 0.01 μm. Noting that the average thickness of the cementite plates in commercial pearlitic rail steels is mostly less than 0.03 μm, it can be conjugated that these cementite plates are fully or mostly plastic (Langford, 1977). Langford (1977) also demonstrated that, in order for pearlite to work harden as it does, lamellar cementite must be ductile, because the generation of the dislocations required in the pile-ups absorbs a significant fraction of the work of deformation. In the following analysis, both cementite and ferrite are assumed to be elastoplastic.

For an initially isotropic and plastically incompressible continuum, an elastoplastic model was proposed by Fan and Peng (1991) under the condition of isothermal and small deformation. It is related to the endochronic plastic constitutive equation (Valanis, 1980), model of Chaboche et al. (1979) and some other constitutive models (Peng et al., 1996; Chaboche, 1986; Watanabe and Atluri, 1986). The corresponding incremental form of the constitutive equation can be expressed as (Peng and Fan, 1993)

$$\Delta\mathbf{s}(z) = A\,\Delta\mathbf{e}^{\mathrm{p}} + \mathbf{B}(z_n)\Delta z, \tag{1}$$

where $\Delta\mathbf{s}$ and $\Delta\mathbf{e}^{\mathrm{p}}$ are the increments of deviatoric stress and plastic strain, respectively,

$$A = \sum_{r=1}^{n} k_r C_r, \qquad \mathbf{B}(z_n) = -\sum_{r=1}^{n} k_r \alpha_r \mathbf{s}^{(r)}(z_n), \tag{2}$$

$$\Delta\mathbf{s}^{(r)}(z) = k_r(C_r\,\Delta\mathbf{e}^{\mathrm{p}} - \alpha_r \mathbf{s}^{(r)}(z_n))\Delta z, \quad k_r = \frac{1 - \mathrm{e}^{-\alpha_r \Delta z}}{\alpha_r \Delta z}, \quad \Delta z = z - z_n, \tag{3}$$

z is generalized time which is non-negative and increases monotonically during any plastic deformation process due to the following definition of Δz:

$$\Delta z = \frac{\Delta\zeta}{f(z)}, \qquad \Delta\zeta^2 = \Delta\mathbf{e}^{\mathrm{p}} : \Delta\mathbf{e}^{\mathrm{p}}, \tag{4}$$

$f(z)$ is a hardening function, C_r and α_r $(r = 1, \ldots, n)$ are material constants. Substituting the incremental form of elastic constitutive equation

$$\Delta\mathbf{e} - \Delta\mathbf{e}^{\mathrm{p}} = \frac{\Delta\mathbf{s}}{2G} \tag{5}$$

into Eq. (1) leads to the following incremental elastoplastic constitutive equation (Peng and Fan, 1993)

$$\Delta\mathbf{s} = 2G_{\mathrm{p}}\,\Delta\mathbf{e} + T_{\mathrm{p}}\mathbf{B}\,\Delta z, \tag{6}$$

where $\mathbf{e}$ denotes deviatoric strain tensor, G is elastic shear modulus, and

$$T_{\mathrm{p}} = \left(1 + \frac{A}{2G}\right)^{-1}, \qquad 2G_{\mathrm{p}} = AT_{\mathrm{p}}. \tag{7}$$

Rewriting Eq. (4) as

$$\Delta z = \frac{\Delta \mathbf{e}^{\mathrm{p}}}{f'^2 \Delta z} : \Delta \mathbf{e}^{\mathrm{p}} \tag{8}$$

and making use of the following relationships

$$\Delta \mathbf{s} = \Delta \boldsymbol{\sigma} - \tfrac{1}{3}\mathrm{tr}(\Delta \boldsymbol{\sigma})\mathbf{I}_2, \qquad \Delta \mathbf{e} = \Delta \boldsymbol{\varepsilon} - \tfrac{1}{3}\mathrm{tr}(\Delta \boldsymbol{\varepsilon})\mathbf{I}_2, \qquad \mathrm{tr}(\Delta \boldsymbol{\sigma}) = 3K\,\mathrm{tr}(\Delta \boldsymbol{\varepsilon}) \tag{9}$$

with $\boldsymbol{\sigma}$ and $\boldsymbol{\varepsilon}$ being respectively stress and strain tensors, K elastic volumetric modulus, and $\mathbf{I}_2$ being the identity tensor of rank two, one can derive the incremental constitutive equation as follows: (Peng and Fan, 1993)

$$\{\Delta\sigma\} = [D]\{\Delta\varepsilon\}, \tag{10}$$

where $[D]$ represents tangential elastoplastic stiffness matrix which consists of two parts:

$$[D] = [D_{\mathrm{e}}] + \frac{2(G - G_{\mathrm{p}})}{H}[D_{\mathrm{p}}]. \tag{11}$$

For a general 3-D problem, these matrices can be expressed as

$$\begin{aligned} \{\Delta\sigma\} &= (\Delta\sigma_{11}, \Delta\sigma_{22}, \Delta\sigma_{33}, \Delta\tau_{12}, \Delta\tau_{23}, \Delta\tau_{31})^{\mathrm{T}}, \\ \{\Delta\varepsilon\} &= (\Delta\varepsilon_{11}, \Delta\varepsilon_{22}, \Delta\varepsilon_{33}, \Delta\gamma_{12}, \Delta\gamma_{23}, \Delta\gamma_{31})^{\mathrm{T}}, \end{aligned} \tag{12}$$

$$[D_{\mathrm{e}}] = \begin{bmatrix} C_1 & C_2 & C_2 & 0 & 0 & 0 \\ C_2 & C_1 & C_2 & 0 & 0 & 0 \\ C_2 & C_2 & C_1 & 0 & 0 & 0 \\ 0 & 0 & 0 & G_{\mathrm{p}} & 0 & 0 \\ 0 & 0 & 0 & 0 & G_{\mathrm{p}} & 0 \\ 0 & 0 & 0 & 0 & 0 & G_{\mathrm{p}} \end{bmatrix}, \tag{13}$$

being an elastic-like matrix,

$$[D_{\mathrm{p}}] = C_3\{\, B_{11} \quad B_{22} \quad B_{33} \quad B_{12} \quad B_{23} \quad B_{31} \,\}^{\mathrm{T}} (\, \Delta e^{\mathrm{p}}_{11} \quad \Delta e^{\mathrm{p}}_{22} \quad \Delta e^{\mathrm{p}}_{33} \quad \Delta e^{\mathrm{p}}_{12} \quad \Delta e^{\mathrm{p}}_{23} \quad \Delta e^{\mathrm{p}}_{31} \,) \tag{14}$$

taking into account the contribution of the history and the current state of plastic strain to $[D]$, and

$$\begin{aligned} C_1 &= K + \tfrac{4}{3}G_{\mathrm{p}}, \qquad C_2 = K - \tfrac{2}{3}G_{\mathrm{p}}, \\ C_3 &= \frac{T_{\mathrm{p}}}{2Gf'^2(z)\Delta z}, \qquad H = 1 + C_3 \mathbf{B} : \Delta \mathbf{e}^{\mathrm{p}}. \end{aligned} \tag{15}$$

3. Constitutive model for a pearlitic colony

A cell of a pearlitic colony is shown in Fig. 2(a), where the white layers represent ferrite lamellas while the black represent cementite ones. It is assumed that all the ferrite and cementite lamellas are parallel with each other, alternatively arranged with perfect bond, and with a constant interlamellar spacing. A coordinate system is fixed on the cell with x_1x_2 plane parallel to the lamellas and x_3 perpendicular to the lamellas. The thickness of each lamella is assumed to be sufficiently small so that the variations of stress and strain in a lamella can be neglected. The in-plane strain components and out-of-plane stress components in all lamellas are, therefore, identical and equal respectively to the corresponding components of the overall strain and stress of the cell to meet the condition of compatibility, i.e.,

$$\mathrm{d}\varepsilon^{\mathrm{c}}_{11} = \mathrm{d}\varepsilon^{\mathrm{f}}_{11} = \mathrm{d}\varepsilon_{11}, \qquad \mathrm{d}\varepsilon^{\mathrm{c}}_{22} = \mathrm{d}\varepsilon^{\mathrm{f}}_{22} = \mathrm{d}\varepsilon_{22}, \qquad \mathrm{d}\gamma^{\mathrm{c}}_{12} = \mathrm{d}\gamma^{\mathrm{f}}_{12} = \mathrm{d}\gamma_{12}, \tag{16}$$

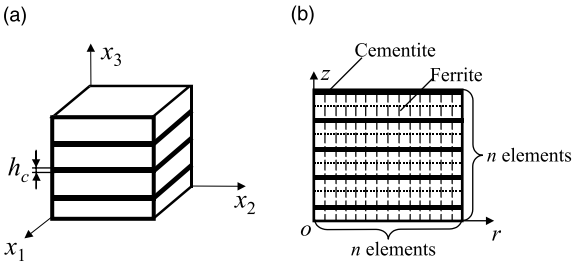

Fig. 2. Lamellar microstructure of a pearlitic colony cell and FE mesh: (a) a cell of a pearlitic colony and (b) FE mesh of the cell.

$$\mathrm{d}\sigma_{33}^{\mathrm{c}} = \mathrm{d}\sigma_{33}^{\mathrm{f}} = \mathrm{d}\sigma_{33}, \qquad \mathrm{d}\tau_{13}^{\mathrm{c}} = \mathrm{d}\tau_{13}^{\mathrm{f}} = \mathrm{d}\tau_{13}, \qquad \mathrm{d}\tau_{23}^{\mathrm{c}} = \mathrm{d}\tau_{23}^{\mathrm{f}} = \mathrm{d}\tau_{23}, \tag{17}$$

where the superscripts c and f represent cementite and ferrite, respectively.

The other components of stress and strain can be determined by volume average as follows:

$$\begin{aligned} \Delta\sigma_{ij} &= V\Delta\sigma_{ij}^{\mathrm{c}} + (1-V)\Delta\sigma_{ij}^{\mathrm{f}}, \quad ij = 11, 22, 12, \\ \Delta\varepsilon_{ij} &= V\Delta\varepsilon_{ij}^{\mathrm{c}} + (1-V)\Delta\varepsilon_{ij}^{\mathrm{f}}, \quad ij = 33, 23, 13, \end{aligned} \tag{18}$$

where V is the volume fraction of cementite. Using Eq. (10), the incremental constitutive equations of cementite and ferrite can be expressed as

$$\{\Delta\sigma^{\mathrm{c}}\} = [D^{\mathrm{c}}]\{\Delta\varepsilon^{\mathrm{c}}\}, \qquad \{\Delta\sigma^{\mathrm{f}}\} = [D^{\mathrm{f}}]\{\Delta\varepsilon^{\mathrm{f}}\}. \tag{19}$$

Substituting Eq. (19) into Eq. (18) yields the following incremental elastoplastic constitutive equation for a pearlitic colony (see Appendix A):

$$\begin{Bmatrix} \Delta\bar{\sigma} \\ \Delta\hat{\sigma} \end{Bmatrix} = \begin{bmatrix} B_2 - B_1 B_3^{-1} B_4 & B_1 B_3^{-1} \\ -B_3^{-1} B_4 & B_3^{-1} \end{bmatrix} \begin{Bmatrix} \Delta\hat{\varepsilon} \\ \Delta\bar{\varepsilon} \end{Bmatrix}, \tag{20}$$

with

$$\begin{aligned} \{\Delta\bar{\sigma}\} &= (\,\Delta\sigma_{11}, \quad \Delta\sigma_{22}, \quad \Delta\tau_{12}\,)^{\mathrm{T}}, \qquad \{\Delta\hat{\sigma}\} = (\,\Delta\sigma_{33}, \quad \Delta\tau_{23}, \quad \Delta\tau_{13}\,)^{\mathrm{T}}, \\ \{\Delta\bar{\varepsilon}\} &= (\,\Delta\varepsilon_{33}, \quad \Delta\gamma_{23}, \quad \Delta\gamma_{13}\,)^{\mathrm{T}}, \qquad \{\Delta\hat{\varepsilon}\} = (\,\Delta\varepsilon_{11}, \quad \Delta\varepsilon_{22}, \quad \Delta\gamma_{12}\,)^{\mathrm{T}}, \end{aligned} \tag{21}$$

$$\begin{aligned} B_1 &= VA_2^{\mathrm{c}}(A_4^{\mathrm{c}})^{-1} + (1-V)A_2^{\mathrm{f}}(A_4^{\mathrm{f}})^{-1}, \\ B_2 &= V[A_1^{\mathrm{c}} - A_2^{\mathrm{c}}(A_4^{\mathrm{c}})^{-1}A_3^{\mathrm{c}}] + (1-V)[A_1^{\mathrm{f}} - A_2^{\mathrm{f}}(A_4^{\mathrm{f}})^{-1}A_3^{\mathrm{f}}], \\ B_3 &= V(A_4^{\mathrm{c}})^{-1} + (1-V)(A_4^{\mathrm{f}})^{-1}, \\ B_4 &= -V(A_4^{\mathrm{c}})^{-1}A_3^{\mathrm{c}} - (1-V)(A_4^{\mathrm{f}})^{-1}A_3^{\mathrm{f}} \end{aligned} \tag{22}$$

and

$$\begin{aligned} [A_1^{\mathrm{c}}] &= \begin{bmatrix} D_{1111}^{\mathrm{c}} & D_{1122}^{\mathrm{c}} & D_{1112}^{\mathrm{c}} \\ D_{2211}^{\mathrm{c}} & D_{2222}^{\mathrm{c}} & D_{2212}^{\mathrm{c}} \\ D_{1211}^{\mathrm{c}} & D_{1222}^{\mathrm{c}} & D_{1212}^{\mathrm{c}} \end{bmatrix}, \qquad [A_2^{\mathrm{c}}] = \begin{bmatrix} D_{1133}^{\mathrm{c}} & D_{1123}^{\mathrm{c}} & D_{1131}^{\mathrm{c}} \\ D_{2233}^{\mathrm{c}} & D_{2223}^{\mathrm{c}} & D_{2231}^{\mathrm{c}} \\ D_{1233}^{\mathrm{c}} & D_{1223}^{\mathrm{c}} & D_{1231}^{\mathrm{c}} \end{bmatrix}, \\ [A_3^{\mathrm{c}}] &= \begin{bmatrix} D_{3311}^{\mathrm{c}} & D_{3322}^{\mathrm{c}} & D_{3312}^{\mathrm{c}} \\ D_{2311}^{\mathrm{c}} & D_{2322}^{\mathrm{c}} & D_{2312}^{\mathrm{c}} \\ D_{3111}^{\mathrm{c}} & D_{3122}^{\mathrm{c}} & D_{3112}^{\mathrm{c}} \end{bmatrix}, \qquad [A_4^{\mathrm{c}}] = \begin{bmatrix} D_{3333}^{\mathrm{c}} & D_{3323}^{\mathrm{c}} & D_{3331}^{\mathrm{c}} \\ D_{2333}^{\mathrm{c}} & D_{2323}^{\mathrm{c}} & D_{2331}^{\mathrm{c}} \\ D_{3133}^{\mathrm{c}} & D_{3123}^{\mathrm{c}} & D_{3131}^{\mathrm{c}} \end{bmatrix}, \end{aligned} \tag{23}$$

where D^{c}_{ijkl} denotes element *ijkl* in the tangential elastoplastic matrix of cementite $[D^{c}]$ (see Eqs. (11), (13), (14) and (19)). Replacing the element D^{c}_{ijkl} with D^{f}_{ijkl} in the tangential elastoplastic matrix of ferrite $[D^{f}]$, one immediately obtains A^{f}_{1} through A^{f}_{4} from Eq. (23).

Eq. (20) describes the overall elastoplastic behavior of a pearlitic colony, which takes into account the microstructure and the cementite volume fraction. It can be seen that the tangential elastoplastic matrix is anisotropic, which is associated with the anisotropic nature of a pearlitic colony. It is important to note that the constitutive description for ferrite and cementite plates in a pearlitic colony can be obtained simultaneously by Eq. (19), giving rise to understand the individual constitutive behavior of each phase.

4. Analysis of the elastoplastic response of a single pearlitic colony

In this section, the responses of a single pearlitic colony subjected to proportional and non-proportional straining, and the cyclic ratcheting under asymmetrical loading are analyzed using the proposed constitutive model.

It has been reported that the elastic properties of both the ferrite and the cementite are almost identical (Langford, 1977) and in the following they are prescribed as

$$E^{c} = E^{f} = E = 210 \text{ GPa}, \qquad G^{c} = G^{f} = G = 80 \text{ GPa},$$

where E^{c} and E^{f} are respectively the Young's moduli of cementite and ferrite, G^{c} and G^{f} are the elastic shear moduli of the two phases, respectively, and E and G are the Young's modulus and the elastic shear modulus of the corresponding pearlitic colony, respectively. According to the assessment of the strengths of ferrite and cementite (Langford, 1977; Park and Bernstein, 1979), the following plastic properties are assumed in the following analysis:

$$C^{f}_{1,2,3} = (450, 80, 4.1) \text{ GPa}, \qquad \alpha^{f}_{1,2,3} = 4000, 420, 74,$$
$$C^{c}_{1,2,3} = (9500, 2800, 650) \text{ GPa}, \qquad \alpha^{c}_{1,2,3} = 50\,000, 3000, 400.$$

For the sake of simplicity without losing generality, the hardening function is assumed to be equal to one for both ferrite and cementite. It can be easily found, for the given material parameters, that the strength of cementite is about seven times that of ferrite. In the following analysis, the volume fraction of cementite V is prescribed as 13%.

The numerical process for a stress-controlled condition can be stated as follows:

(a) With the results obtained by the kth iteration of the ith increment of loading, the tangential elastoplastic matrices $[D^{c}]$ and $[D^{f}]$ can be obtained using Eq. (11).
(b) Calculate B_i $(i = 1, 2, 3, 4)$ by Eq. (22), and then elastoplastic matrix of a pearlitic colony $[D]$ by Eq. (20).
(c) For a given increment of overall stress $\{\Delta\sigma\}$, the corresponding increment of overall strain $\{\Delta\varepsilon\}$ can be determined by solving Eq. (20).
(d) The increments of the unknown stress and strain components for the cementite and ferrite $\{\Delta\bar{\sigma}^{c}\}$, $\{\Delta\bar{\sigma}^{f}\}$, $\{\Delta\bar{\varepsilon}^{c}\}$ and $\{\Delta\bar{\varepsilon}^{f}\}$ can then be respectively derived using Eqs. (A.4) and (A.5).
(e) For cementite, the incremental deviatoric stress $\{\Delta s^{c}\}$ and strain $\{\Delta e^{c}\}$, the generalized time increment $\Delta\zeta^{c}$ and the hardening function $f^{c}(z^{c})$ as well as Δz^{c} can be calculated by Eq. (4). For ferrite, the corresponding quantities can be obtained similarly.
(f) Calculating $\{\Delta s^{(r)c}\}$ and $\{\Delta s^{(r)f}\}$ by Eq. (3) and modifying $\{B^{c}\}$ and $\{B^{f}\}$ by Eq. (2), respectively.
(g) If the following defined error δ is less than the tolerance δ_0, i.e.,

$$\delta = \max\left[\left|\frac{\Delta z_i^k - \Delta z_i^{k-1}}{\Delta z_i^k}\right|_{\mathrm{c}}, \quad \left|\frac{\Delta z_i^k - \Delta z_i^{k-1}}{\Delta z_i^k}\right|_{\mathrm{f}}\right] \leqslant \delta_0,$$

then the iteration for the ith increment of loading is terminated. After modifying the corresponding quantities, one starts the next increment of loading.

For a strain-controlled condition, the similar algorithm can be performed without difficulty.

Fig. 3 shows the response of a single pearlitic colony subjected to ε_{11} (tensile strain in x_1 direction). It is known from Eq. (16) that the ferrite and cementite lamellas undergo an identical strain ε_{11}, and their responses are also shown in Fig. 3. The maximum stress in ferrite is only around 435 MPa, while in the case of cementite, this value is clearly higher, i.e., 3374 MPa. The saturated stress of the pearlitic colony is about 819 MPa, being easily obtained by Eq. (18).

The response of a single pearlitic colony subjected to uniaxial strain ε_{33} (tensile strain in x_3 direction) is given in Fig. 4. Computation shows that the overall saturated value of σ_{33} in the pearlitic colony is also about 819 MPa, which is approximately identical with the saturated value of σ_{11} corresponding to the uniaxial strain ε_{11} (Fig. 3). In this direction, the tensile stresses in the ferrite and cementite are almost identical with the overall stress component σ_{33}, i.e., $\sigma_{33}^{\mathrm{f}} = \sigma_{33}^{\mathrm{c}} = \sigma_{33} = 819$ MPa (Eq. (17)). It has already

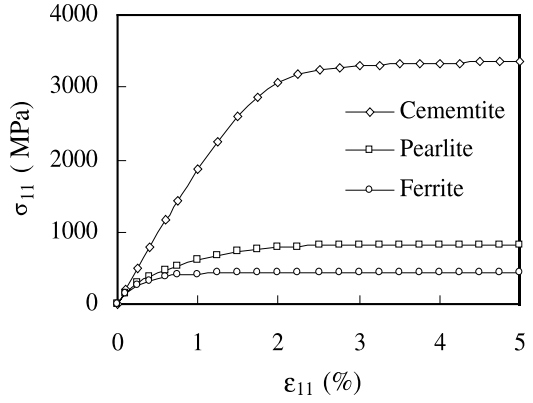

Fig. 3. Response of a single pearlitic colony subjected to uniaxial strain ε_{11}.

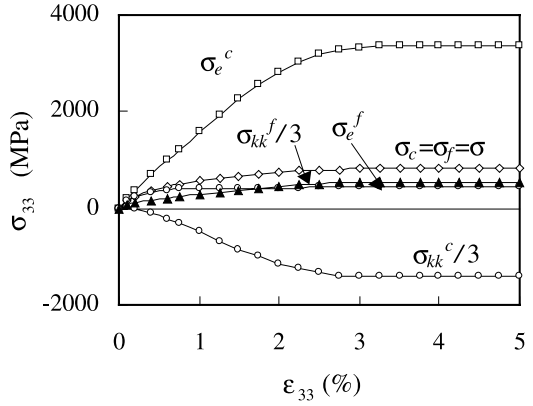

Fig. 4. Response of a single pearlitic colony subjected to uniaxial strain ε_{33}.

greatly exceeded the tensile strength of ferrite. Detailed analysis shows that in this case the equivalent stresses σ_e^f and σ_e^c in the ferrite and cementite are respectively 435 and 3374 MPa (Fig. 4). These magnitudes are similar to those related to uniaxial strain ε_{11}. But, the volumetric stresses σ_{kk}^f and σ_{kk}^c, in both phases are 1585 and -4287 MPa (Fig. 4), respectively. This is quite different from those in the colony subjected to uniaxial strain ε_{11}, where the volumetric stresses in both the ferrite and cementite phases are identical to the values of σ_{11}^f and σ_{11}^c. Although the existence of the tensile volumetric stress increases the load-baring capability of ferrite to some extent, it increases the risk of the initiation and growth of damage. If the single pearlitic colony is compressed in x_3 direction, the volumetric stresses in ferrite will become negative while that in cementite positive. The compressive volumetric stress helps reducing damage in ferrite, while the tensile volumetric stress in cementite may be acceptable because of the much higher strength of cementite, which accounts for the extensive application of pearlitic steel as rail steel.

When a single pearlitic colony is subjected to pure shear strain γ_{13}, computation shows that the saturated shear stress $\tau_{13}^f = \tau_{13}^c = \tau_{13} = 253$ MPa, and the saturated equivalent stress is 437 Pa (Fig. 5), being just the strength of ferrite. It indicates that when a single pearlitic colony is subjected to γ_{13}, its strength is solely determined by the strength of ferrite. The relationship between the equivalent stress and strain of the colony subjected respectively to γ_{12} is also shown in Fig. 5. In this case, the saturated equivalent stress is about 819 MPa, being the combination of the strengths of ferrite and cementite by their volume fractions (Eq. (17)). The comparison between the two shear stress–strain responses indicates the anisotropy of the pearlitic colony.

In order to study the anisotropic property of a single pearlitic colony, the stress responses along 90° out-of-phase circular paths in the planes of ε_{11}–$\gamma_{12}/\sqrt{3}$, ε_{11}–$\gamma_{13}/\sqrt{3}$ and ε_{33}–$\gamma_{13}/\sqrt{3}$ (Fig. 6(a)) are investigated, respectively. The radius of the circular strain paths is 0.03. Fig. 6(b) shows respectively the stress loci in the corresponding σ–$\sqrt{3}\tau$ planes. It can be seen that the stress locus in the σ_{11}–$\sqrt{3}\tau_{12}$ plane is nearly a circle, which coincides with the isotropic property in this plane of the colony (Fig. 2(a)). Compared with the above response, the stress locus σ_{11}–$\sqrt{3}\tau_{13}$ corresponding to the circular path in ε_{11}–$\gamma_{13}/\sqrt{3}$ plane shows marked anisotropy. So does the stress locus σ_{33}–$\sqrt{3}\tau_{13}$ corresponding to the circular path in ε_{33}–$\gamma_{13}/\sqrt{3}$ plane. Marked difference between the stress loci σ_{11}–$\sqrt{3}\tau_{13}$ and σ_{33}–$\sqrt{3}\tau_{13}$ can also be detected. It, again, indicates the anisotropy of the overall responses of the pearlitic colony.

The variation of the ratcheting rate of the single pearlitic colony subjected to asymmetrical cyclic stress σ_{11} is numerically investigated under plane-strain condition ($\varepsilon_{22} \equiv 0$). Fig. 7(a) shows σ_{11}–ε_{11} evolution where σ_{11} varies between -100 and 600 MPa (with mean stress 250 MPa and stress amplitude 350 MPa). It can be seen that the accumulated plastic strain $(\varepsilon_{11})_{accu}$ increases as the stress cycling proceeds, but its rate

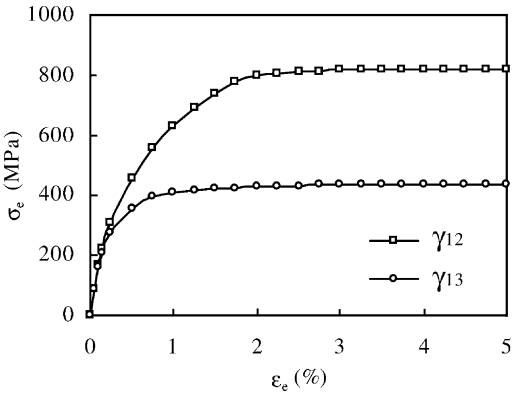

Fig. 5. Response of a single pearlitic colony subjected to shear strain γ_{12} and γ_{13}, respectively.

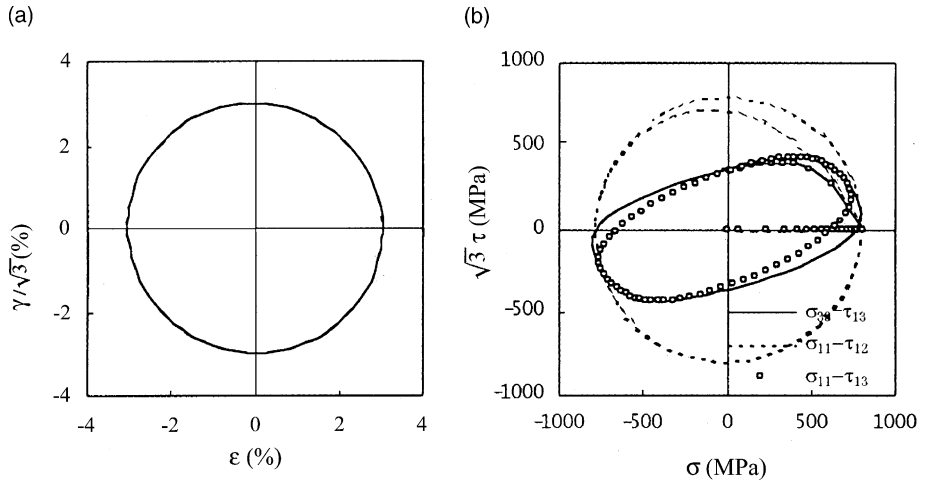

Fig. 6. Responses along circular paths in different ε–$\gamma/\sqrt{3}$ planes: (a) 90° out-of-phase circular strain path and (b) stress loci in σ–$\sqrt{3}\tau$ planes.

$(\mathrm{d}\varepsilon_{11})_{\mathrm{accu}}/\mathrm{d}N$ gradually decreases (Fig. 7(b)), which qualitatively coincides with the observation in the experiment of pearlitic rail steel (Peng and Ponter, 1994b). It is known that during the asymmetrical cyclic stress, the redistribution of the mean stress in both phases determines the ratcheting state. If the cementite (hard phase) is fully elastic, the ratcheting will stop when the accumulated strain is sufficiently large, so that the cementite can take over all the mean stress and the ferrite will be solely subjected to symmetric cyclic stressing (Peng and Ponter, 1994b). If the cementite is elastoplastic, as assumed in this work, the situation becomes complicated and the redistribution of the mean stress is determined by the elastoplastic properties of both phases. Fig. 9(a) shows the variation of the mean deviatoric stresses in both ferrite and cementite phases ignoring the volumetric stress that does not contribute to accumulated strain. It can be seen that the mean deviatoric stress in the ferrite decreases and tends to vanish, but the mean deviatoric stress in cementite s^{c}_{11} is much larger and governs the ratcheting rate in the cyclic process. The decrease of s^{c}_{11} during cyclic process may account for the decrease of the ratcheting rate.

Fig. 8(a) shows the relationship between σ_{33} and ε_{33} where σ_{33} varies between -100 and 600 MPa (250 ± 350 MPa) under plane-strain condition ($\varepsilon_{22} \equiv 0$). It can be seen that the response in this case is similar to that one in the x_1 direction as shown in Fig. 7. The variation of the mean deviatoric stress in the ferrite is smaller to that shown in Fig. 9(a). The mean deviatoric stress in the cementite increases and approaches to a steady value, which implies the corresponding steady state of ratcheting.

5. FEM simulation

The relationships in Eqs. (16)–(18) were obtained based on the assumption of very fine lamellas. In order to demonstrate the validity of the above approach, the responses of pearlitic colonies with different interlamellar spacing are analyzed with finite element method.

The response of the pearlitic colony subjected to tensile strain ε_{33} is analyzed. For simplicity, the pearlitic colony is assumed to be a cylinder and its axis is perpendicular to the lamellas, the radius and the interlamellar spacing of the cylinder are denoted by R and a, respectively. Axisymmetrical finite element code is used. Due to symmetry, the upper-right quarter of the vertical section of the cylinder was adopted for the analysis (Fig. 2(b)). It is further separated into $n \times n$ elements with $(n+1)^2$ nodes in total.

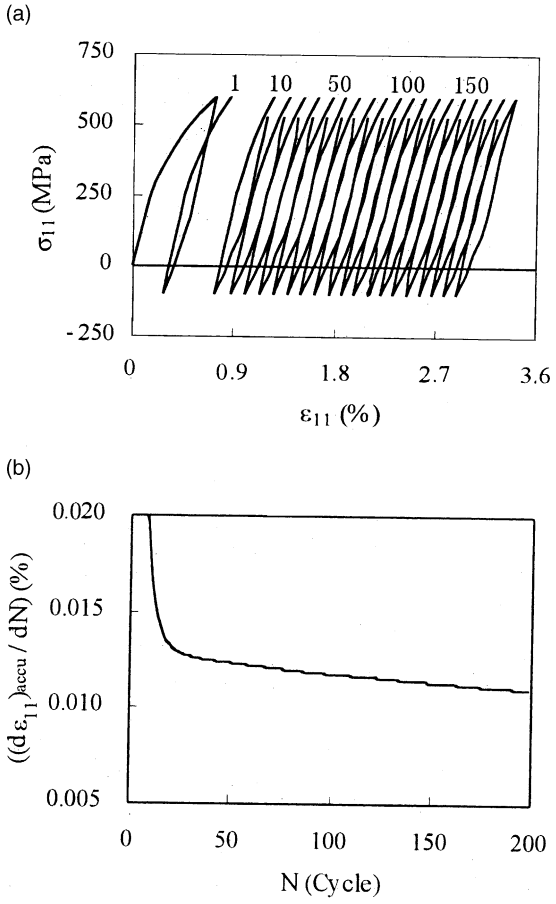

Fig. 7. Cyclic ratcheting in ε_{11} direction: (a) cyclic σ_{11}–ε_{11} curve and (b) variation of $(\mathrm{d}\varepsilon_{11})_{\mathrm{accu}}/\mathrm{d}N$.

The numbers of lamellas used in computation were 7, 11, 15 and 19, and the corresponding n was 5, 8, 11 and 14, respectively. Uniform vertical displacement is prescribed to each of the upper nodes. The average saturated stress σ_{33} is defined as the ratio between the overall saturated vertical load and the area of the cross-section.

The effect of the number of lamellas on the stress response of the pearlitic colony with $R/a \approx 58$ (or $\log(a/R) \approx -1.76$) is shown in Fig. 10(a). It is obvious that the average saturated stress σ_{33} is over predicted if the number of the used lamellas is small. σ_{33} decreases with the increasing number of lamellas and approaches an asymptotic value when the number of lamellas is sufficiently large. It is shown in Fig. 10(a) that the proposed microstructure-based model provides this asymptotic value and the result by FEM simulation is quite close to this value when 19 lamellas is used.

The effect of the interlamellar spacing a and the radius of lamellas R on the saturated stress is given in Fig. 10(b). One can conclude that the larger the interlamellar spacing, the smaller is the saturated stress. If the interlamellar spacing is sufficiently large, i.e., the thickness of a ferrite lamella is sufficiently large, the saturated stress σ_{33} is governed by the strength of ferrite. σ_{33} tends to the value obtained by the microstructure-based model (see Fig. 4) when the interlamellar spacing is sufficiently small. If the number of lamellas is 15, $\sigma_{33} = 825$ MPa when $\log(a/R) = -1.76$, which is very close to the magnitude of

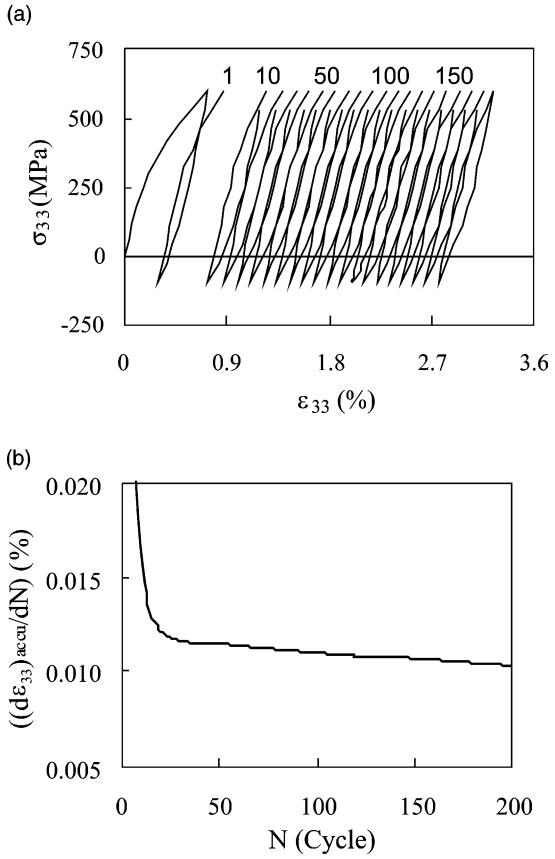

Fig. 8. Cyclic ratcheting in ε_{33} direction: (a) cyclic σ_{33}–ε_{33} curve and (b) variation of $(\mathrm{d}\varepsilon_{33})_{\mathrm{accu}}/\mathrm{d}N$.

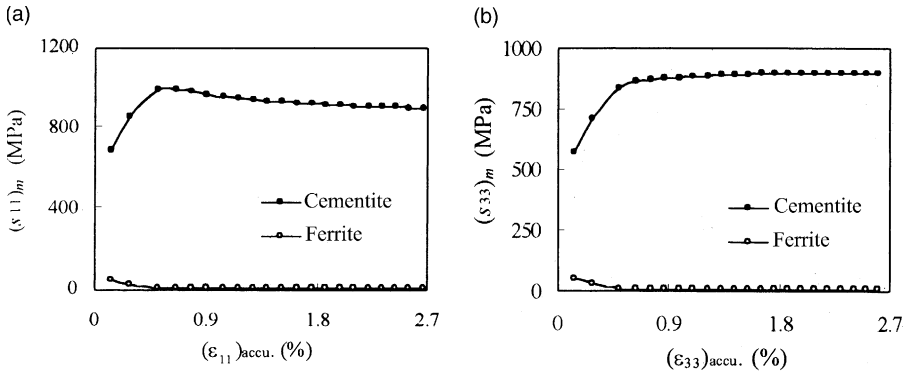

Fig. 9. Variations of the deviatoric stress in both phases versus accumulated strain: (a) variations of $(s_{11})_m$ and (b) variations of $(s_{33})_m$.

819 MPa obtained with the proposed model. If the size of a pearlitic colony $R = 13$ μm, the corresponding a can be determined as 270 nm, which is much larger than the interlamellar spacing of that in either on-line

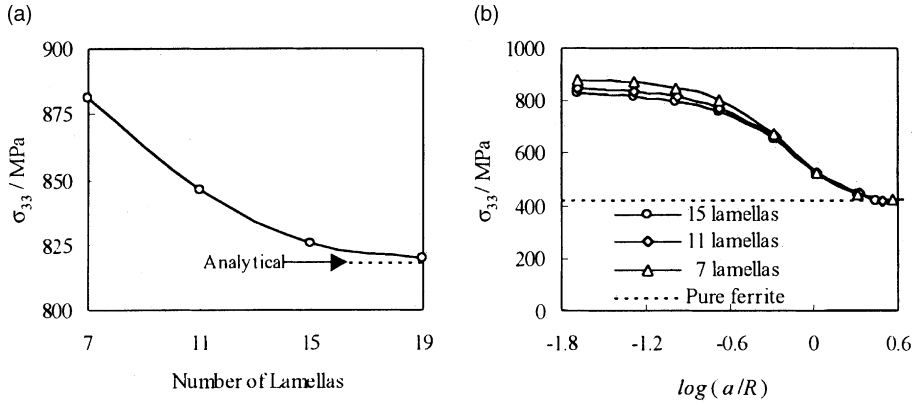

Fig. 10. FEM simulation for the response of pearlitic colonies: (a) effect of the adopted number of lamellas and (b) effect of the interlamellar spacing.

and full-length quenched rail steel ($a = 136$ nm) or hot-rolled rail steel ($a = 190$ nm). It demonstrates the validity of proposed constitutive description in the application to the constitutive response of pearlitic rail steel.

6. Conclusions

A pearlitic colony is composed of many thin lamellas of ferrite and cementite, its mechanical behavior can be determined by its microstructure and the mechanical property of each phase. Based on this concept, a constitutive description was obtained for a single pearlitic colony with the assumptions that the interlamellar spacing is sufficiently small and, both ferrite and cementite are elastoplastic.

The responses of the single pearlitic colony were analyzed. It was found that under uniaxial strain in the directions parallel to and perpendicular to the lamellas, the overall responses look similar but the stress states are substantially different. In the latter case, larger volumetric stresses exist in both phases due to the interaction between them. It, on one hand, may increase the overall strength, but on the other hand, may induce damage in the ferrite. Analysis showed that compressive load results in more satisfactory stress states in both phases, which accounts for the extensive use of such kind of materials as in rail steel. Comparison between the responses of a single pearlitic colony under various proportional and non-proportional loading shows distinct anisotropy.

When the colony is subjected to asymmetrical cyclic stress σ_{11} or σ_{33}, it ratchets in the direction of mean stress with decreasing rate. The mean deviatoric stress in ferrite phase tends to vanish, while that in cementite phase is kept at a high level, which governs the ratcheting of the pearlitic colony.

Finite element analysis was conducted to demonstrate the validity of the proposed approach. It was shown that the proposed approach provides the asymptotic result as the interlamellar spacing is sufficiently small and the number of lamellas is sufficiently large. It showed that the proposed approach could describe with sufficient accuracy the constitutive behavior of the colony with moderate interlamellar spacing.

The constitutive response of each phase in a pearlitic colony can be obtained simultaneously, which is an important step towards developing theories of a microstructure-based damage and failure analysis. The proposed approach is also significant to the analysis of the constitutive behavior of pearlitic steel, which is regarded as an aggregate of numerous pearlitic colonies with randomly distributed orientations.

Acknowledgements

The authors gratefully acknowledge the financial support to this work from the Natural Science Foundation of China and the Education Ministry of China.

Appendix A

Noticing the relationships shown in Eqs. (16) and (17), applying Eq. (10) to cementite gives

$$\begin{Bmatrix} \Delta\sigma^{c}_{11} \\ \Delta\sigma^{c}_{22} \\ \Delta\tau^{c}_{12} \\ \Delta\sigma^{c}_{33} \\ \Delta\tau^{c}_{23} \\ \Delta\tau^{c}_{31} \end{Bmatrix} = \begin{bmatrix} D^{c}_{1111} & D^{c}_{1122} & D^{c}_{1112} & D^{c}_{1133} & D^{c}_{1123} & D^{c}_{1131} \\ D^{c}_{2211} & D^{c}_{2222} & D^{c}_{2212} & D^{c}_{2233} & D^{c}_{2223} & D^{c}_{2231} \\ D^{c}_{1211} & D^{c}_{1222} & D^{c}_{1212} & D^{c}_{1233} & D^{c}_{1223} & D^{c}_{1231} \\ D^{c}_{3311} & D^{c}_{3322} & D^{c}_{3312} & D^{c}_{3333} & D^{c}_{3323} & D^{c}_{3331} \\ D^{c}_{2311} & D^{c}_{2322} & D^{c}_{2312} & D^{c}_{2333} & D^{c}_{2323} & D^{c}_{2331} \\ D^{c}_{3111} & D^{c}_{3122} & D^{c}_{3112} & D^{c}_{3133} & D^{c}_{3123} & D^{c}_{3131} \end{bmatrix} \begin{Bmatrix} \Delta\varepsilon^{c}_{11} \\ \Delta\varepsilon^{c}_{22} \\ \Delta\gamma^{c}_{12} \\ \Delta\varepsilon^{c}_{33} \\ \Delta\gamma^{c}_{23} \\ \Delta\gamma^{c}_{31} \end{Bmatrix}. \tag{A.1}$$

Eq. (A.1) can be rewritten in the following laconic form

$$\begin{Bmatrix} \Delta\bar{\sigma}^{c} \\ \Delta\hat{\sigma}^{c} \end{Bmatrix} = \begin{bmatrix} A^{c}_{1} & A^{c}_{2} \\ A^{c}_{3} & A^{c}_{4} \end{bmatrix} \begin{Bmatrix} \Delta\hat{\varepsilon}^{c} \\ \Delta\bar{\varepsilon}^{c} \end{Bmatrix} \tag{A.2}$$

in which

$$\begin{aligned} \{\Delta\bar{\sigma}^{c}\} &= \left(\Delta\sigma^{c}_{11}, \Delta\sigma^{c}_{22}, \Delta\tau^{c}_{12}\right)^{T}, \qquad \{\Delta\hat{\sigma}^{c}\} = \left(\Delta\sigma^{c}_{33}, \Delta\tau^{c}_{23}, \Delta\tau^{c}_{31}\right)^{T}, \\ \{\Delta\hat{\varepsilon}^{c}\} &= \left(\Delta\varepsilon^{c}_{11}, \Delta\varepsilon^{c}_{22}, \Delta\gamma^{c}_{12}\right)^{T}, \qquad \{\Delta\bar{\varepsilon}^{c}\} = \left(\Delta\varepsilon^{c}_{33}, \Delta\gamma^{c}_{23}, \Delta\gamma^{c}_{31}\right)^{T}, \end{aligned} \tag{A.3}$$

and A^{c}_{1}, A^{c}_{2}, A^{c}_{3} and A^{c}_{4} are shown in Eq. (23). It can easily be solved from Eq. (A.1) that

$$\begin{Bmatrix} \Delta\bar{\sigma}^{c} \\ \Delta\bar{\varepsilon}^{c} \end{Bmatrix} = \begin{bmatrix} A^{c}_{2}(A^{c}_{4})^{-1} & A^{c}_{1} - A^{c}_{2}(A^{c}_{4})^{-1}A^{c}_{3} \\ (A^{c}_{4})^{-1} & -(A^{c}_{4})^{-1}A^{c}_{3} \end{bmatrix} \begin{Bmatrix} \Delta\hat{\sigma} \\ \Delta\hat{\varepsilon} \end{Bmatrix}. \tag{A.4}$$

Replacing superscript "c" with "f" one obtains the following expression for ferrite:

$$\begin{Bmatrix} \Delta\bar{\sigma}^{f} \\ \Delta\bar{\varepsilon}^{f} \end{Bmatrix} = \begin{bmatrix} A^{f}_{2}(A^{f}_{4})^{-1} & A^{f}_{1} - A^{f}_{2}(A^{f}_{4})^{-1}A^{f}_{3} \\ (A^{f}_{4})^{-1} & -(A^{f}_{4})^{-1}A^{f}_{3} \end{bmatrix} \begin{Bmatrix} \Delta\hat{\sigma} \\ \Delta\hat{\varepsilon} \end{Bmatrix}. \tag{A.5}$$

Making use of Eq. (18) one can obtain the following relationship:

$$\begin{Bmatrix} \Delta\bar{\sigma} \\ \Delta\bar{\varepsilon} \end{Bmatrix} = V\begin{Bmatrix} \Delta\bar{\sigma}^{c} \\ \Delta\bar{\varepsilon}^{c} \end{Bmatrix} + (1-V)\begin{Bmatrix} \Delta\bar{\sigma}^{f} \\ \Delta\bar{\varepsilon}^{f} \end{Bmatrix} = \begin{bmatrix} B_{1} & B_{2} \\ B_{3} & B_{4} \end{bmatrix} \begin{Bmatrix} \Delta\hat{\sigma} \\ \Delta\hat{\varepsilon} \end{Bmatrix}, \tag{A.6}$$

where B_1, B_2, B_3 and B_4 are shown in Eq. (22). Eq. (A.6) can be rewritten as

$$\Delta\bar{\sigma} = B_1\,\Delta\hat{\sigma} + B_2\,\Delta\hat{\varepsilon}, \qquad \Delta\bar{\varepsilon} = B_3\,\Delta\hat{\sigma} + B_4\,\Delta\hat{\varepsilon}. \tag{A.7}$$

It can be solved from Eq. (A.7) that

$$\Delta\hat{\sigma} = B_3^{-1}\,\Delta\bar{\varepsilon} - B_3^{-1}B_4\,\Delta\hat{\varepsilon}, \qquad \Delta\bar{\sigma} = B_1B_3^{-1}\,\Delta\bar{\varepsilon} - (B_1B_3^{-1}B_4 - B_2)\Delta\hat{\varepsilon}, \tag{A.8}$$

which is just Eq. (20).

References

Armstrong, R.J., Frederick, C.O., 1966. A mathematical representation of the multiaxial Bauschinger effect, CEGB, Report/RD/B/N 731, General Electricity Generating Board.

Bower, A.F., 1987. The influence of strain hardening on cumulative plastic deformation caused by repeated rolling and sliding contact. University of Cambridge, CUED/C-Mech/TR.39.

Bower, A.F., 1989. Cyclic hardening properties of hard-drawn copper and rail steel. J. Mech. Phys. Solids 37, 455–470.

Bower, A.F., Johnson, K.L., 1989. The influence strain hardening on cumulative plastic deformation in rolling and sliding contact. J. Mech. Phys. Solids 37, 471–493.

Bower, A.F., Johnson, K.L., 1990. Plastic flow and shakedown of rail surface in repeated wheel-rail contact. 3rd Int. Symp. Contact Mech. & Wear of Wheel-Rail Systems, Cambridge, UK.

Chaboche, J.L., Dang, V.K., Gordier, G., 1979. Modelization of strain effect on the cyclic hardening of 316 stainless steel. Trans. Int. Conf. Struct. Mech. Reactor Tech., Paper No. L11/3, V.L., Berlin.

Chaboche, J.L., 1986. Time-dependent constitutive theories for cyclic plasticity. Int. J. Plast. 2, 149–188.

Clayton, P., 1980. The relation between wear behavior and basic material properties for pearlitic steels. Wear 60, 75–93.

Fan, J., 1999. A micro/macroscopic analysis for cyclic plasticity of dual-phase materials. J. Appl. Mech. 66, 124–136.

Fan, J., Peng, X., 1991. A physically based constitutive description for nonproportional cyclic plasticity. J. Engng. Mater. Technol. 113, 254–262.

Hodson, W.H., Preston, R.R., 1980. Production processes to yield superior rail steel. Trans. Res. Pec., 1744–1754.

Langford, G., 1977. Deformation of Pearlite. Metall. Trans. A. 8A, 861–875.

Park, Y.J., Bernstein, I.M., 1979. The process of crack initiation and effective grain size for cleavage fracture in pearlitic eutectoid steel. Metall. Trans. A. 10A, 1653–1663.

Peng, X., Fan, J., 1993. A numerical approach for nonclassical plasticity. Comput. Struct. 47, 313–320.

Peng, X., Ponter, A.R.S., 1994a. A constitutive law for a class of two-phase materials with experimental verification. Int. J. Solids Struct. 31, 1099–1111.

Peng, X., Ponter, A.R.S., 1994b. An experimental investigation of the response of BS11 steel to cyclic loading. Int. J. Solids Struct. 31, 807–833.

Peng, X., Fan, J., Zeng, X., 1996. Analysis for plastic buckling of thin-walled cylinder via non-classical constitutive theory of plasticity. Int. J. Solids Struct. 33, 4495–4509.

Petez-Unzueta, A.J., Beynon, J.H., 1995. Microstructure and wear resistance of pearlitic rail steels. Wear 144, 172–182.

Sheng, G., Fan, J., Peng, X., Jiang, B., Ji, K., Su, S., Ke, X., 1998. Investigation of contact fatigue behaviors of PD_3 rail steel. Steel Iron 33, 35–39 (in Chinese).

Valanis, K.C., 1980. Fundamental consequences of new intrinsic time measure plasticity as a limit of the endochronic theory. Arch. Mech. 23, 171–190.

Watanabe, O., Atluri, S.N., 1986. Internal time, general internal variable, and multiyield-surface theories of plasticity and creep. Int. J. Plast. 2, 37–52.